Geophysical Research Letters

RESEARCH LETTER
10.1029/2019GL083166

Modeling Contributions of Continents and Oceans to the Diurnal Variation of the Global Electric Circuit

Nikolay N. Slyunyaev, Nikolay V. Ilin, and Evgeny A. Mareev

Institute of Applied Physics, Russian Academy of Sciences, Nizhny Novgorod, Russia

Key Points:
- Diurnal variation of the global electric circuit is simulated with the WRF model using a new parameterization of the ionospheric potential
- Model predicts maximum contributions to the global electric circuit at 14:00–18:00 LT for continents and at 2:00–6:00 LT for oceans
- Contributions from ocean regions with many islands (Maritime Continent and Middle America) have maxima at both 14:00–18:00 and 2:00–6:00 LT

Correspondence to:
N. N. Slyunyaev,
slyunyaev.n@gmail.com

Citation:
Slyunyaev, N. N., Ilin, N. V., & Mareev, E. A. (2019). Modeling contributions of continents and oceans to the diurnal variation of the global electric circuit. *Geophysical Research Letters*, *46*, 5516–5525. https://doi.org/10.1029/2019GL083166

Received 3 APR 2019
Accepted 26 APR 2019
Accepted article online 1 MAY 2019
Published online 20 MAY 2019

Abstract Contributions of different land and ocean regions to the diurnal variation of the global electric circuit are simulated using the Weather Research and Forecasting model by estimating the ionospheric potential produced by thunderstorms and electrified shower clouds in each grid column. The model predicts that contributions from land regions have maxima at about 14:00–18:00 local time (LT), whereas contributions from oceans have maxima at about 2:00–6:00 LT, and different ocean regions show nearly the same relative diurnal variation. It is remarkable that contributions from ocean regions with many islands (Maritime Continent and Middle America) have maxima at both 14:00–18:00 and 2:00–6:00 LT.

1. Introduction

According to the concept of the global electric circuit (GEC), the distribution of electric fields and currents in the entire atmosphere is primarily determined by the processes occurring in electrified clouds (e.g., Rycroft et al., 2008; Williams & Mareev, 2014). Charge separation inside thunderstorms and electrified shower clouds (ESCs) maintains a global network of quasi-stationary currents (direct current GEC, or DC GEC), whereas lightning excites the Schumann resonances in the Earth-ionosphere cavity (alternating current GEC, or AC GEC). Since noninductive charging, which is believed to be dominant in electrified clouds, is associated with intense convection, it is clear that the GEC variations should reflect weather and climate changes (e.g., Markson, 2007; Williams, 2009).

Investigating the diurnal cycle of atmospheric electricity facilitates understanding this relationship between the GEC and weather. Over the past few years, the interest in studying the diurnal variation of atmospheric electrical parameters has been increasing; recent progress in this direction is related to satellite and aircraft cloud observations (Liu et al., 2010; Mach et al., 2011; Peterson et al., 2017), analyzing the data of global lightning locating systems (Hutchins et al., 2014; Mezuman et al., 2014), and using weather and climate models to simulate DC GEC parameters (Jánský et al., 2017; Kalb et al., 2016; Mareev & Volodin, 2014) and distribution of lightning flashes (Romps et al., 2018).

It has long been established that the diurnal variation of DC GEC parameters (the so-called Carnegie curve; see Harrison, 2013) is similar to the diurnal variation of global thunderstorm activity (Whipple & Scrase, 1936), which confirms the idea that quasi-stationary currents in the atmosphere are driven by electrified clouds. The shape of the Carnegie curve is usually interpreted as the result of superposition of diurnal cycles of thunderstorm activity over different continents (Markson, 2007), which are known to have pronounced maxima at about 15:00–17:00 local time (LT; Bailey et al., 2007). This interpretation motivates further research aimed at analyzing regional contributions to the diurnal variation of the GEC.

Here we focus on the DC GEC and study its diurnal variation by considering one of its most fundamental characteristics, namely, the ionospheric potential (IP), defined as the potential of the ionosphere relative to the Earth's surface. We parameterize the IP in the globally running Weather Research and Forecasting model (WRF) by estimating contributions to the total IP produced by model grid columns in terms of climate variables, thus generalizing the parameterization of Mareev and Volodin (2014). This approach allows us to make use of the advantages of weather forecasting models, which are able to simulate atmospheric dynamics using meteorological data, for investigating the important problem of theoretical reproduction of the GEC. The focus on the IP makes it possible to analyze diurnal variations of contributions to the GEC from different land and ocean regions. There have been only few attempts to reproduce GEC variation in models of atmospheric dynamics (Jánský et al., 2017; Lucas et al., 2015; Mareev & Volodin, 2014); however, previous modeling studies did not consistently address the problem of regional contributions, dealing with few regions bounded by large rectangles or even just by meridians; here we for the first time simulate and discuss regional contributions in detail, emphasizing the contrast of atmospheric dynamics above land and ocean.

2. Model and Parameterization

2.1. Modeling the Atmospheric Dynamics

We simulate atmospheric dynamics using the WRF running globally (https://www.mmm.ucar.edu/weather-research-and-forecasting-model; Powers et al., 2017; Skamarock et al., 2008); more precisely, we use version 3.9.1 of the Advanced Research WRF. We use a $1° \times 1°$ latitude-longitude grid with 51 altitude levels from the Earth's surface to the 10-mbar level and time steps of 150 s. We choose the following set of physics schemes for the WRF model: mp_physics = 2, ra_lw_physics = 4, ra_sw_physics = 4, radt = 30, sf_sfclay_physics = 1, sf_surface_physics = 2, bl_pbl_physics = 1, and cu_physics = 2. Precipitation is calculated on the basis of the parameterization of convection (so-called convective rain). The National Centers for Environmental Prediction Global Data Assimilation System/final results of operational global analysis and forecast on a $0.25° \times 0.25°$ grid data set (NCEP GDAS/FNL 0.25; https://rda.ucar.edu/datasets/ds083.3) is used to initialize the WRF model.

2.2. Parameterizing the IP

To parameterize the IP in the WRF model, we generally follow the approach underlying the parameterization of Mareev and Volodin (2014). Since the diurnal variation of the GEC is primarily determined by the variation of its sources, we can neglect the Earth's orography and assume that the conductivity σ depends only on the altitude above sea level z. In this case one can express the IP analytically (Kalinin et al., 2014, eq. (31)) as

$$V = \iint \frac{j_z^{\mathrm{s}}(z, \lambda, \psi)}{S_{\mathrm{E}}\sigma(z)} \, \mathrm{d}z \, \mathrm{d}S, \tag{1}$$

where j_z^{s} is the vertical component of the charge separation (source) current density, S_{E} is the total area of the Earth's surface, and λ and ψ are the latitude and longitude in radians, respectively; the outer integral in (1) is taken over the Earth's surface, whereas the inner one is taken over the altitude range containing electrified clouds.

To rewrite (1) for the WRF, we replace the outer integration with summation over grid columns consisting of grid cells with the same latitude and longitude. We make the following assumptions:

1. We approximate the lower and upper boundaries of the mixed phase region of electrified clouds in the ith grid column, z_i^{l} and z_i^{u}, with the heights of the 0 and −38 °C isotherms, respectively (more precisely, with the heights of the nearest grid levels above them). This is the region where charge separation occurs in case of noninductive charging.
2. We assume the area covered by electrified clouds in the ith column to be proportional to $S_i P_i / W_i$, where S_i is the total area of the column, W_i is the amount of precipitable water stored in the column, and P_i is the amount of precipitation totaled over the symmetric 2-hr period around the moment that W_i is computed. This parameterization represents the assumption that in the presence of convection, an air parcel precipitates almost all the water that it contains during its ascent, in which case the ratio of the amount of water precipitated during the corresponding time interval to W_i estimates the portion of the column area where convection occurs and, by inference, where electrified clouds develop. Although the 2-hr time interval that we use for calculating P_i is somewhat longer than typical air ascent times, analysis shows that changing the length of this time interval does not affect the resulting relative diurnal variation substantially.
3. We assume constant charge separation current density j_z^{s} inside the mixed phase region of electrified clouds in those grid columns where convective available potential energy (CAPE) exceeds $\varepsilon_0 = 1$ kJ/kg and $j_z^{\mathrm{s}} = 0$ otherwise, thus taking into account the fact that electrified clouds, which alone contribute to the GEC, are mostly characterized by deep convection (we calculate CAPE with the function cape_2d of the wrf-python package, which estimates the maximum value of CAPE in each grid column; see https://wrf-python.readthedocs.io/en/latest/user_api/generated/wrf.cape_2d.html). Analysis shows that threshold CAPE values in the range between 0.6 and 1.2 kJ/kg yield similar relative IP variations, and $\varepsilon_0 = 1$ kJ/kg is chosen since this value gives slightly better agreement with the classical Carnegie curve than the other ones.

4. We assume an exponential conductivity profile, namely, $\sigma(z) = \sigma_0 \exp(z/H)$ with $H = 6$ km; this is a characteristic scale height chosen on the basis of analyzing more elaborate conductivity parameterizations of Tinsley and Zhou (2006) and Slyunyaev et al. (2015).

Assumptions 1–4 allow us to rewrite (1) as

$$V = \sum_i \frac{j_0 H S_i}{\sigma_0 S_{\mathrm{E}}} \frac{P_i}{W_i} \left(\exp\left(-\frac{z_i^{\mathrm{l}}}{H}\right) - \exp\left(-\frac{z_i^{\mathrm{u}}}{H}\right) \right) \times \begin{cases} 0, & \varepsilon_i < \varepsilon_0, \\ 1, & \varepsilon_i \geq \varepsilon_0, \end{cases} \quad (2)$$

where ε_i is the maximum value of CAPE in the ith grid column, j_0 is a constant, and the summation takes place over all grid columns.

Equation (2) also allows us to estimate contributions to the IP from different regions: To this end, we just restrict the summation to the grid columns lying within respective regions. Note that regional contributions to the Wilson current are equal to the corresponding contributions to the IP divided by the resistance of the entire fair-weather part of the GEC and thus have the same diurnal cycles.

2.3. Simulating the Diurnal Variation of the IP

To simulate the diurnal variation of the IP, we perform 732 48-hr free runs of the WRF starting at 0:00 and 12:00 UTC on every day from 31 December 2015 to 30 December 2016. In each model run we calculate the IP every hour by equation (2). The results over the first several hours since the model initiation are not reliable, as the model needs some time to achieve the correct reproduction of the data absent in initial conditions (e.g., precipitation); therefore, we restrict our attention to the time interval between 18 and 42 hr since the model initiation and consider two 24-hr data sets representing the IP evolution over this time interval, (i) the average of the 366 model runs initiated at 0:00 UTC and (ii) the average of the 366 model runs initiated at 12:00 UTC. Clearly, these data sets correspond to the 24-hr intervals starting and ending at 18:00 and at 6:00 UTC, respectively.

Although the IP variations obtained in model runs starting at 0:00 and 12:00 UTC are quasiperiodic, neither of them exactly repeats itself after 24 hr. To obtain a periodic diurnal variation, we use the following "regularization" procedure. First we make each of the two data sets described above periodic by linearly adjusting IP values while keeping the mean value of the IP the same. After this adjustment we have two 24-hr periodic data sets representing the IP evolution, one of them starting and ending at 18:00 UTC and the other starting and ending at 6:00 UTC. After appropriate shifting both these data sets represent the diurnal variation of the IP, and we take the average of these two variations as the final result.

3. Results and Discussion

3.1. Contributions of Continents and Oceans to the GEC

We consider contributions to the GEC produced by thunderstorms and ESCs over different continents and oceans; to this purpose, we divide the entire Earth's surface (including the oceans) into 14 regions, as shown in Figure 1a. These regions correspond to large parts of continents (together with strips of surrounding water) and oceans; we emphasize that labels used for different regions in Figure 1a do not strictly correspond to exact geographical terms (e.g., "Africa" contains the Arabian peninsula, "Europe" includes part of western and central Asia etc.).

Figures 2a and 2b show diurnal variations of contributions to the IP from different land and ocean regions obtained using equation (2). Europe and northern Asia are combined, considering that their separate contributions are too small to be shown at this scale. The contribution of polar regions is not included at all, inasmuch as it is extremely small; this is not surprising, for convective activity in these regions is negligible (see Figure 1b, showing the geographical distribution of mean annual CAPE values). By comparing individual plots in Figures 2a and 2b, we see that absolute values of regional contributions differ substantially; South America produces the largest contribution to the IP among land regions, while the western Pacific Ocean gives the largest contribution among oceanic regions.

In Figures 2c and 2d the contributions of land and ocean regions to the IP are shown cumulatively. Their sum, shown in Figure 2e, has the same shape as the classical Carnegie curve, known from electric field observations and shown in Figure 2f (after Harrison, 2013), although with maxima shifted by about 2 hr and with about 46% smaller peak-to-peak amplitude (18% of the mean against 34% of the mean). Since Figures 2c and 2d imply that contributions of land regions have larger relative peak-to-peak variation than those of

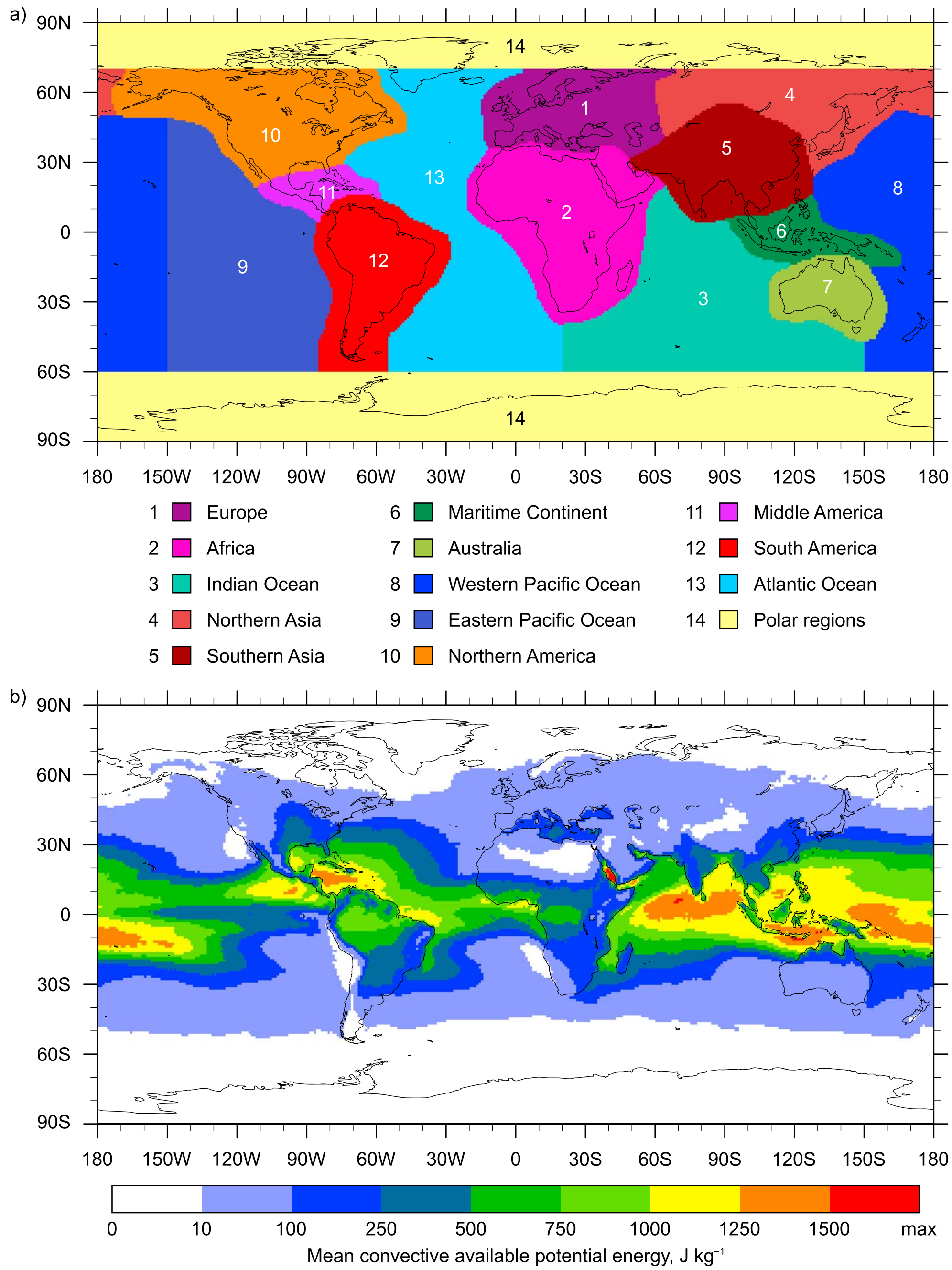

Figure 1. (a) Partition of the Earth's surface into regions for analyzing contributions to the ionospheric potential. (b) Mean annual values of maximum convective available potential energy.

oceans (54% and 7% of the respective means), it is likely that IP parameterizations based on convection overestimate ocean contributions, for Mareev and Volodin (2014) and Jánský et al. (2017) obtained peak-to-peak amplitudes of the same order when using convection to parameterize GEC source currents in climate models. Note that our IP parameterization reproduces the shape of the classical Carnegie curve better than those used in previous studies in that it correctly predicts one minimum and two maxima within 1 or 2 hr of the real ones.

3.2. Relative Contributions of Continents and Oceans in Local Time

To better understand the nature of regional contributions to the IP, it is convenient to transfer Figures 2a and 2b to local times and represent individual contributions as fractions of their own means rather than of

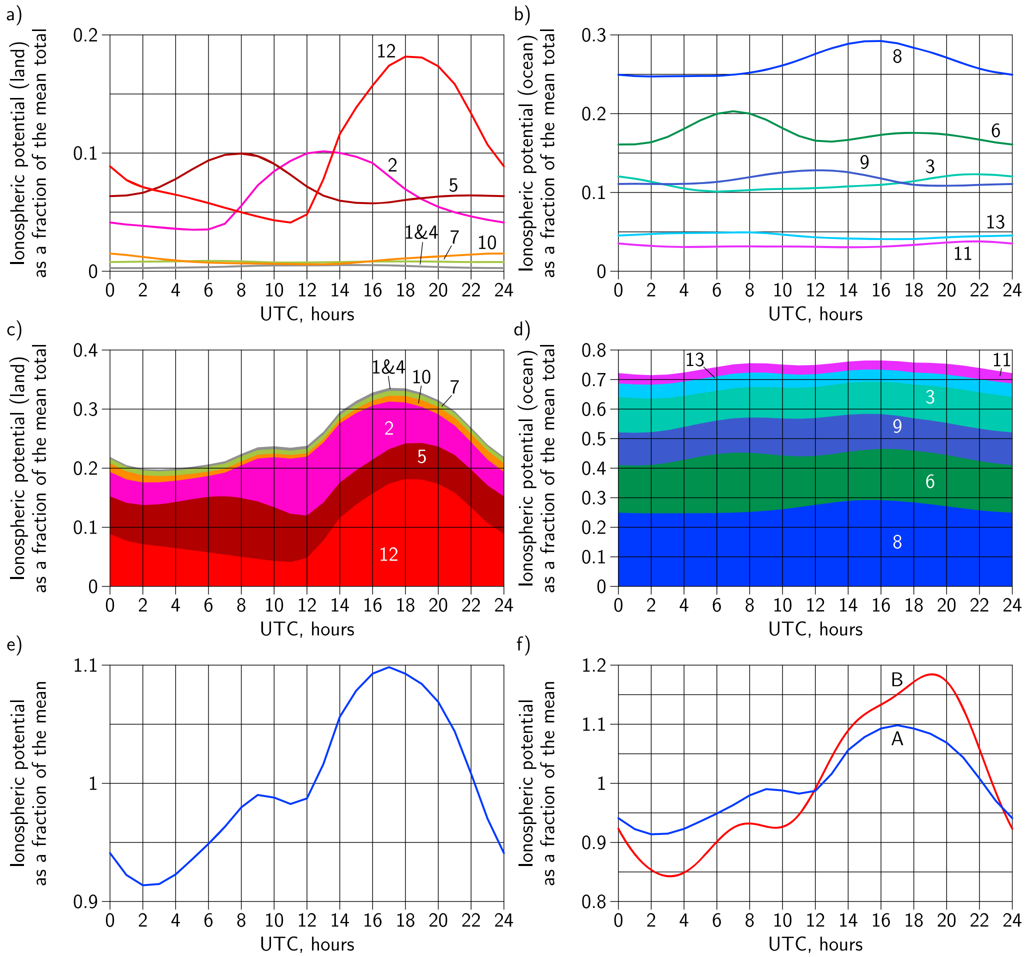

Figure 2. (a) Simulated diurnal variations of contributions of different land regions to the IP. (b) Simulated diurnal variations of contributions of different ocean regions (including the Maritime Continent and Middle America, which are not purely oceanic areas) to the IP. (c) Panel (a) in cumulative representation. (d) Panel (b) in cumulative representation. (e) Simulated diurnal variation of the total IP. (f) Simulated diurnal variation of the total IP (A) and the classical Carnegie curve (B, after Harrison, 2013). In panels (a)–(d) the colors and labels are chosen according to Figure 1a, except for gray in panels (a) and (c), which represents the sum of contributions from Europe and northern Asia. The contribution from polar regions is not shown, given that it is extremely small. All contributions to the IP are shown as fractions of the mean total. IP = ionospheric potential.

the mean total. Figure 3a shows relative IP variations for land regions in local time, which is computed on the basis of average longitude. According to our simulations, contributions of all land regions have pronounced maxima between 14 and 18 LT, except for northern Asia, whose contribution reaches its maximum slightly later (note, however, that the absolute value of this contribution is rather small in comparison with others, as Figure 2a shows). Figure 3b shows relative IP variations for ocean regions in local time. Contributions of purely oceanic regions have pronounced maxima between 2 and 6 LT; it is remarkable that whereas relative IP variations for land regions differ significantly, their counterparts for purely oceanic regions are more or less similar.

In our partition of the Earth's surface (Figure 1a) there are two ocean regions with many large islands, namely, the Maritime Continent and Middle America. It is remarkable that the behavior of contributions of these regions to the IP variation is, in a sense, intermediate between those of contributions from pure land and oceans: According to Figure 3b, they have primary maxima at about 15–17 LT (corresponding to land) and secondary maxima at about 2–3 LT (corresponding to oceans). It is even more striking that two different regions of this type, the Maritime Continent and Middle America, have very close relative IP variations in spite of the great distance separating them (note also that the contribution of Australia, shown in Figure 3a, behaves in a somewhat similar way).

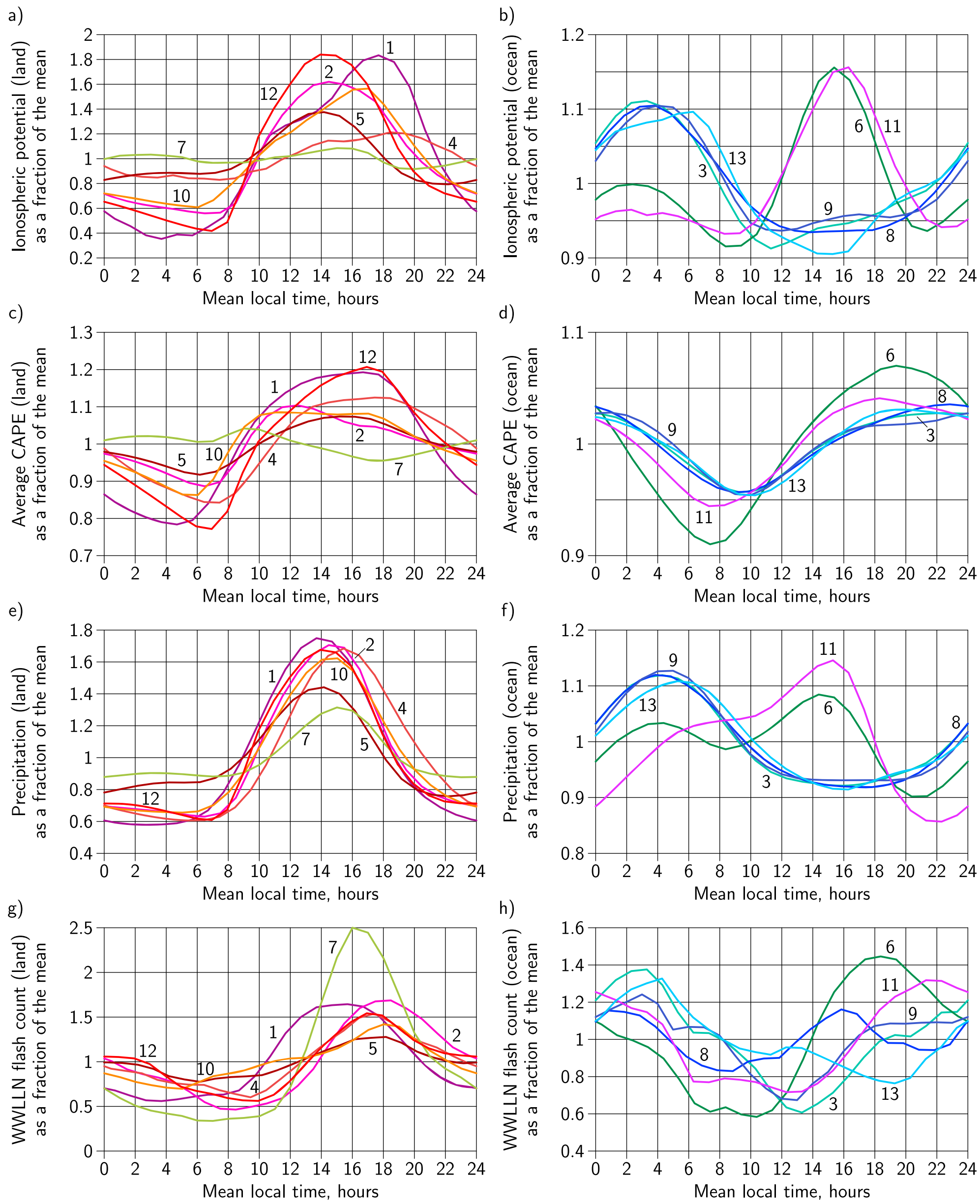

Figure 3. (a) Simulated diurnal variations of contributions of land regions to the IP. (b) Simulated diurnal variations of contributions of ocean regions (including the Maritime Continent and Middle America) to the IP. (c) Simulated diurnal variations of average CAPE over land regions. (d) Simulated diurnal variations of average CAPE over ocean regions. (e) Simulated diurnal variations of precipitation rate over land regions. (f) Simulated diurnal variations of precipitation rate over ocean regions. (g) Diurnal variations of WWLLN flash counts over land regions. (h) Diurnal variations of WWLLN flash counts over ocean regions. All quantities are shown as fractions of regional means rather than the mean total, and in all eight panels mean local times are used instead of UTC. The colors and labels are chosen according to Figure 1a. CAPE = convective available potential energy; IP = ionospheric potential; WWLLN = World Wide Lightning Location Network.

3.3. Comparison With CAPE Values and Precipitation Rates

The IP parameterization described in section 2.2 is based on estimating CAPE and precipitation intensity for each grid column (although equation (2) also involves the amount of precipitable water and cloud geometry, calculations show that these factors do not significantly affect the resulting IP variation). Relative variations of average CAPE values and precipitation rates (calculated on the basis of symmetric 2-hr intervals) for different land and ocean regions in local time are shown in Figures 3c–3f; to obtain periodic variations, we use the same "regularization" procedure as that described in section 2.3 for the IP. Note that the positions of diurnal maxima of average CAPE (Figures 3c and 3d) and precipitation rate (Figures 3e and 3f) typically differ by several hours (it is interesting that for purely oceanic regions, maxima and minima of average CAPE occur when precipitation rates are nearly equal to their daily means, and vice versa).

It is clear that diurnal maxima of the IP in our simulations are primarily determined by precipitation rate maxima, which is a manifestation of the relationship existing between atmospheric electricity and rainfall (cf. Liu et al., 2010; Price, 2009). We should note, however, that we use precipitation estimated from the parameterization of convection, since models of the atmospheric dynamics with large-scale grids are not able to faithfully represent cloud microphysics; therefore, in our study both CAPE and precipitation intensity, in a sense, characterize convective activity. Notwithstanding this fact, observations (e.g., Gray & Jacobson, 1977) and satellite data (e.g., Imaoka & Spencer, 2000) confirm that precipitation over oceans indeed peaks at early morning.

It is not hard to find a physical interpretation for the land-ocean contrast observed in simulated diurnal cycles of CAPE (Figures 3c and 3d), precipitation rate (Figures 3e and 3f), and the IP (Figures 3a and 3b). Now that water is mobile and has about 4 times higher heat capacity than land, the air over land takes less time to heat up, and convection over land regions develops faster; daytime sea breezes and nighttime land breezes caused by the difference in the heating of land and ocean also contribute to the development of convection. Therefore, it is not surprising that convective activity over land attains its maximum in the late afternoon, while convection over oceans peaks at night, which eventually determines the land-ocean contrast in the positions of IP maxima.

3.4. Comparison With Lightning Flash Counts

Now that both lightning discharges and quasi-stationary currents of the GEC are manifestations of electrical activity in the atmosphere (largely due to convection), it is not surprising that diurnal variations of the electric field or IP (the Carnegie curve) and thunderstorm or lightning activity are often considered in close connection with each other (see, e.g., Harrison, 2013; Nickolaenko et al., 2006), although notable difference between the two variations has also been pointed out (e.g., Hutchins et al., 2014; Mach et al., 2011; Mezuman et al., 2014; Williams & Heckman, 1993; Williams & Mareev, 2014). It is interesting to compare simulated regional contributions to the IP with the corresponding lightning flash counts. Figures 3g and 3h demonstrate average diurnal variations of lightning flash counts for the regions specified in Figure 1a, according to the data of the World Wide Lightning Location Network (WWLLN) for the year 2016 (a 1-hr time step is used). Direct comparison of WWLLN flash counts for different regions has little sense in view of the fact that WWLLN stations cover the Earth's surface inhomogeneously (Virts et al., 2013). However, we restrict our attention to the comparison of relative variations in local time, which should not be critically affected by this deficiency.

Relative WWLLN flash counts over land regions (Figure 3g) have maxima at approximately the same hours as the IP (14–18 LT), which more or less agrees with 15–17 LT reported by Bailey et al. (2007). The behavior of relative WWLLN flash counts over purely oceanic regions (Figure 3h) is more complicated (especially in the case of the western Pacific Ocean), but maxima at about 2–6 LT corresponding to those of the IP are also clearly seen. At the same time diurnal cycles of WWLLN flash counts for the two ocean regions with many large islands (Figure 3h) do not have second maxima corresponding to those of the IP (they are probably dominated by land contributions, but this issue requires a more careful analysis involving land and sea breezes, which are particularly important in such regions).

According to the analysis of Williams et al. (2000), global variations in lightning activity are primarily caused by changes in the number of thunderstorms rather than by the variation of the mean flash rate. The IP parameterization used in this study employs a somewhat similar assumption: The same source current density is ascribed to every electrified cloud, and the IP variation is primarily determined by the variation of the area occupied by these clouds (estimated on the basis of simulated CAPE and precipitation intensity). Considering this fact, as well as the existence of a strong positive correlation between the Wilson current produced by a thunderstorm and the corresponding lightning flash rate (LFR), found by Blakeslee et al. (1989), it is not surprising that regional contributions to the IP (proportional to the Wilson current) and LFR in many aspects show similar behavior.

However, strictly speaking, regional contributions to the GEC and LFR are not unambiguously related. The difference between the GEC variation and the LFR variation may be attributed to the variance in the number of ESCs over different regions and to the effects of aerosols, which may influence both charge separation currents and LFR and whose content also varies across the Earth's surface; however, we do not consider aerosols in this study.

3.5. Further Discussion

As we have noted above, the difference between GEC and LFR variations may, to a large extent, be related to the fact that ESCs, not possessing lightning activity, contribute to the GEC along with thunderstorms. According to the analysis of satellite observations by Peterson et al. (2018), thunderstorms supply about 61% of the total current to the GEC, while ESCs provide the remaining 39%; earlier estimates of Mach et al. (2011) on the basis of aircraft observations give a smaller ESC contribution to the GEC, but those results are likely to be subject to a sampling bias.

In this study we do not distinguish between thunderstorms and ESCs, as we believe that IP parameterizations based on convection take into account both types of electrified clouds. Moreover, large-scale models of weather and climate are not able to resolve individual clouds, and it is not clear how one could separate grid columns occupied by thunderstorms from those occupied by ESCs on the basis of climate variables alone. In any case, although it is usually thought that land thunderstorms, oceanic thunderstorms, land ESCs, and oceanic ESCs supply different mean currents to the GEC (Mach et al., 2011), the relationships between the corresponding current densities are less clear, and it is difficult to find a physically based parameterization for the source current densities corresponding to electrified clouds of different types. Therefore, IP parameterizations that treat all electrified clouds in the same way are acceptable as the simplest approximation of the real situation and presently seem the most reliable from a physical perspective.

A more important issue related to the inability of large-scale models of atmospheric dynamics to distinguish thunderstorms from ESCs is the uncertainty of such models in separating electrified clouds from nonelectrified ones, which do not contribute to the GEC at all. We have already noted that IP parameterizations based on convection tend to overestimate the contribution of oceans. This happens because the criteria used to single out electrified clouds on the basis of convective activity alone are rather rough; more precise criteria require using cloud microphysics and small-scale grids. Despite this limitation, comparison of the simulated IP variation (Figure 2e) with the classical Carnegie curve (Figure 2f) allows us to expect that our simulation correctly predicts relative diurnal cycles of contributions to the IP from different regions. The results of this study emphasize the contrast existing between land and ocean regions in the context of atmospheric electricity.

It is interesting that recently Romps et al. (2014) have suggested an LFR parameterization based on the product of CAPE and precipitation; they found that this parameterization predicts the geographical distribution and diurnal cycle of lightning over land (they mostly investigated the contiguous United States) but does not show the pronounced land-ocean contrast in LFR (Romps et al., 2018). From a physical viewpoint, it seems that the product of CAPE and precipitation is more likely to characterize charging currents and the IP than LFR, for it does not distinguish thunderstorms from ESCs. Although in this study we use another expression for the IP, it is based on similar ideas, as contributions from grid columns in equation (2) are proportional to the product of a step function depending on CAPE and the area covered by electrified clouds, estimated using the amount of precipitation. Considering that parameterizations of both IP and LFR based on convection seem to overestimate ocean contributions, the relationship between GEC parameters and LFR requires additional investigation, especially over oceans.

4. Conclusions

The IP can be parameterized in weather forecasting and climate models by estimating the contributions produced by thunderstorms and ESCs in each grid column on the basis of convection and precipitation. Having developed such a parameterization for the WRF model, we obtained the IP variation whose shape is nearly identical to that of the classical Carnegie curve, albeit with a smaller peak-to-peak amplitude and slightly shifted maxima and minima, which is probably caused by the uncertainty in distinguishing electrified clouds from nonelectrified ones in large-scale models and agrees with the results of other similar studies.

The model predicts that contributions from land regions have maxima at about 14:00–18:00 LT, whereas contributions from pure oceans have maxima at about 2:00–6:00 LT, and different ocean regions show nearly the same relative diurnal variation. It is interesting that contributions from ocean regions with many islands

(Maritime Continent and Middle America), according to the model, have maxima at both 14:00–18:00 and 2:00–6:00 LT. The land-ocean contrast in the IP behavior is apparently caused by the difference in the development of convection over land and oceans.

Acknowledgments

The authors are grateful to E. M. Volodin for useful discussions and to the two reviewers of this paper for valuable recommendations. This work was supported by the Russian Science Foundation (project 18-77-10061). The WRF-ARW model is available at http://www2.mmm.ucar.edu/wrf/users/downloads.html; the NCEP GDAS/FNL 0.25 data set is available at the website (https://rda.ucar.edu/datasets/ds083.3). The complete description of simulation options, IP parameterization, and procedures used to compute the mean IP is given in section 2 (division of the Earth's surface into regions, scripts, and results are available at https://bitbucket.org/nilyin/grl2019). WWLLN data can be obtained through the website (http://wwlln.net).

References

Bailey, J. C., Blakeslee, R. J., Buechler, D. E., & Christian, H. J. (2007). Diurnal lightning distributions as observed by the Optical Transient Detector (OTD) and the Lightning Imaging Sensor (LIS). In *13th Int. Conf. on Atmospheric Electricity*, Beijing.

Blakeslee, R. J., Christian, H. J., & Vonnegut, B. (1989). Electrical measurements over thunderstorms. *Journal of Geophysical Research*, *94*(D11), 13,135–13,140. https://doi.org/10.1029/JD094iD11p13135

Gray, W. M., & Jacobson, R. W. (1977). Diurnal variation of deep cumulus convection. *Monthly Weather Review*, *105*(9), 1171–1188. https://doi.org/1520-0493(1977)105<1171:DVODCC>2.0.CO;2

Harrison, R. G. (2013). The Carnegie curve. *Surveys in Geophysics*, *34*(2), 209–232. https://doi.org/10.1007/s10712-012-9210-2

Hutchins, M. L., Holzworth, R. H., & Brundell, J. B. (2014). Diurnal variation of the global electric circuit from clustered thunderstorms. *Journal of Geophysical Research: Space Physics*, *119*, 620–629. https://doi.org/10.1002/2013JA019593

Imaoka, K., & Spencer, R. W. (2000). Diurnal variation of precipitation over the tropical oceans observed by TRMM/TMI combined with SSM/I. *Journal of Climate*, *13*(23), 4149–4158. https://doi.org/10.1175/1520-0442(2000)013<4149:DVOPOT>2.0.CO;2

Jánský, J., Lucas, G. M., Kalb, C., Bayona, V., Peterson, M. J., Deierling, W., et al. (2017). Analysis of the diurnal variation of the global electric circuit obtained from different numerical models. *Journal of Geophysical Research: Atmospheres*, *122*, 12,906–12,917. https://doi.org/10.1002/2017JD026515

Kalb, C., Deierling, W., Baumgaertner, A., Peterson, M., Liu, C., & Mach, D. (2016). Parameterizing total storm conduction currents in the Community Earth System Model. *Journal of Geophysical Research: Atmospheres*, *121*, 13,715–13,734. https://doi.org/10.1002/2016JD025376

Kalinin, A. V., Slyunyaev, N. N., Mareev, E. A., & Zhidkov, A. A. (2014). Stationary and nonstationary models of the global electric circuit: Well-posedness, analytical relations, and numerical implementation. *Izvestiya, Atmospheric and Oceanic Physics*, *50*(3), 314–322. https://doi.org/10.1134/S0001433814030074

Liu, C., Williams, E. R., Zipser, E. J., & Burns, G. (2010). Diurnal variations of global thunderstorms and electrified shower clouds and their contribution to the global electrical circuit. *Journal of the Atmospheric Sciences*, *67*(2), 309–323. https://doi.org/10.1175/2009JAS3248.1

Lucas, G. M., Baumgaertner, A. J. G., & Thayer, J. P. (2015). A global electric circuit model within a community climate model. *Journal of Geophysical Research: Atmospheres*, *120*, 12,054–12,066. https://doi.org/10.1002/2015JD023562

Mach, D. M., Blakeslee, R. J., & Bateman, M. G. (2011). Global electric circuit implications of combined aircraft storm electric current measurements and satellite-based diurnal lightning statistics. *Journal of Geophysical Research*, *116*, D05201. https://doi.org/10.1029/2010JD014462

Mareev, E. A., & Volodin, E. M. (2014). Variation of the global electric circuit and ionospheric potential in a general circulation model. *Geophysical Research Letters*, *41*, 9009–9016. https://doi.org/10.1002/2014GL062352

Markson, R. (2007). The global circuit intensity: Its measurement and variation over the last 50 years. *Bulletin of the American Meteorological Society*, *88*(2), 223–241. https://doi.org/10.1175/BAMS-88-2-223

Mezuman, K., Price, C., & Galanti, E. (2014). On the spatial and temporal distribution of global thunderstorm cells. *Environmental Research Letters*, *9*(12), 124023. https://doi.org/10.1088/1748-9326/9/12/124023

Nickolaenko, A. P., Hayakawa, M., & Sekiguchi, M. (2006). Variations in global thunderstorm activity inferred from the OTD records. *Geophysical Research Letters*, *33*, l06823. https://doi.org/10.1029/2005GL024884

Peterson, M., Deierling, W., Liu, C., Mach, D., & Kalb, C. (2017). A TRMM/GPM retrieval of the total mean generator current for the global electric circuit. *Journal of Geophysical Research: Atmospheres*, *122*, 10,025–10,049. https://doi.org/10.1002/2016JD026336

Peterson, M., Deierling, W., Liu, C., Mach, D., & Kalb, C. (2018). A TRMM assessment of the composition of the generator current that supplies the global electric circuit. *Journal of Geophysical Research: Atmospheres*, *123*, 8208–8220. https://doi.org/10.1029/2018JD028844

Powers, J. G., Klemp, J. B., Skamarock, W. C., Davis, C. A., Dudhia, J., Gill, D. O., et al. (2017). The Weather Research and Forecasting Model: Overview, system efforts, and future directions. *Bulletin of the American Meteorological Society*, *98*(8), 1717–1737. https://doi.org/10.1175/BAMS-D-15-00308.1

Price, C. (2009). Will a drier climate result in more lightning? *Atmospheric Research*, *91*(2–4), 479–484. https://doi.org/10.1016/j.atmosres.2008.05.016

Romps, D. M., Charn, A. B., Holzworth, R. H., Lawrence, W. E., Molinari, J., & Vollaro, D. (2018). CAPE times *P* explains lightning over land but not the land-ocean contrast. *Geophysical Research Letters*, *45*, 12,623–12,630. https://doi.org/10.1029/2018GL080267

Romps, D. M., Seeley, J. T., Vollaro, D., & Molinari, J. (2014). Projected increase in lightning strikes in the United States due to global warming. *Science*, *346*(6211), 851–854. https://doi.org/10.1126/science.1259100

Rycroft, M. J., Harrison, R. G., Nicoll, K. A., & Mareev, E. A. (2008). An overview of Earth's global electric circuit and atmospheric conductivity. *Space Science Reviews*, *137*(1–4), 83–105. https://doi.org/10.1007/s11214-008-9368-6

Skamarock, W. C., Klemp, J. B., Dudhia, J., Gill, D. O., Barker, D., Duda, M. G., et al. (2008). A description of the Advanced Research WRF version 3 (*NCAR Technical Note NCAR/TN-475+STR*). https://doi.org/10.5065/D68S4MVH

Slyunyaev, N. N., Mareev, E. A., & Zhidkov, A. A. (2015). On the variation of the ionospheric potential due to large-scale radioactivity enhancement and solar activity. *Journal of Geophysical Research: Space Physics*, *120*, 7060–7082. https://doi.org/10.1002/2015JA021039

Tinsley, B. A., & Zhou, L. (2006). Initial results of a global circuit model with variable stratospheric and tropospheric aerosols. *Journal of Geophysical Research*, *111*, D16205. https://doi.org/10.1029/2005JD006988

Virts, K. S., Wallace, J. M., Hutchins, M. L., & Holzworth, R. H. (2013). Highlights of a new ground-based, hourly global lightning climatology. *Bulletin of the American Meteorological Society*, *94*(9), 1381–1391. https://doi.org/10.1175/BAMS-D-12-00082.1

Whipple, F. J. W., & Scrase, F. J. (1936). *Point discharge in the electric field of the Earth: An analysis of continuous records obtained at Kew Observatory*. London: H. M. Stationery Off. Geophys. Mem. No. 68.

Williams, E. R. (2009). The global electrical circuit: A review. *Atmospheric Research*, *91*(2–4), 140–152. https://doi.org/10.1016/j.atmosres.2008.05.018

Williams, E. R., & Heckman, S. J. (1993). The local diurnal variation of cloud electrification and the global diurnal variation of negative charge on the Earth. *Journal of Geophysical Research*, *98*(D3), 5221–5234. https://doi.org/10.1029/92JD02642

Williams, E., & Mareev, E. (2014). Recent progress on the global electrical circuit. *Atmospheric Research*, *135–136*, 208–227. https://doi.org/10.1016/j.atmosres.2013.05.015

Williams, E., Rothkin, K., Stevenson, D., & Boccippio, D. (2000). Global lightning variations caused by changes in thunderstorm flash rate and by changes in the number of thunderstorms. *Journal of Applied Meteorology*, *39*(12), 2223–2230. https://doi.org/10.1175/1520-0450(2001)040<2223:GLVCBC>2.0.CO;2